AEM Accepted Manuscript Posted Online 7 May 2021
Appl Environ Microbiol doi:10.1128/AEM.00286-21

Revised Manuscript: AEM00286-21

Oxygen generation via water splitting by a novel biogenic metal ion binding compound

Philip Dershwitz[1], Nathan L. Bandow[1Ψ], Junwon Yang[2], Jeremy D. Semrau[2], Marcus T. McEllistrem[3], Rafael A. Heinze[3], Matheus Fonseca[3], Joshua C. Ledesma[1], Jacob R. Jennett[1], Ana M. DiSpirito[1], Navjot S. Athwal[1ϒ], Mark S. Hargrove[1], Thomas A. Bobik[1], Hans Zischka[4], and Alan A. DiSpirito[1]*

[1]Roy J. Carver Department of Biochemistry, Biophysics and Molecular Biology. Iowa State University, Ames, IA 50011-3260, USA

[2]Department of Civil and Environmental Engineering, University of Michigan, Ann Arbor, MI, 48109-2125, USA

[3]Materials Science and Biomedical Engineering, University of Wisconsin-Eau Claire, WI, 54602, USA

[4] Institute of Molecular Toxicology and Pharmacology, Helmholtz Center Munich, German Research Center for Environmental Health, Ingolstaedter Landstrasse 1, D-85764 Neuherberg, Germany. and Technical University Munich, School of Medicine, Institute of Toxicology and Environmental Hygiene, Biedersteiner Strasse 29, D-80802 Munich, Germany.

[Ψ] Current address: Allogene Therapeutics, Inc., South San Francisco, CA 94080, USA

[ϒ]Current address: Stemcell Technologies, Vancouver, BC Canada

*To whom correspondence should be addressed: Email: aland@iastate.edu; Phone: 1-515-294-2944; Fax: 1-515-294-0453

Running title: Oxidation of water by methanobactin

Keywords: Methanobactin • chalkophore• water oxidation • methanotroph • aerobic methane oxidation • gold nanoparticle.

ABSTRACT

Methanobactins (MBs) are small (<1,300 Da) post-translationally modified copper-binding peptides and represent the extracellular component of a copper acquisition system in some methanotrophs. Interestingly, MBs can bind a range of metal ions, with some reduced after binding, e.g., Cu^{2+} reduced to Cu^{+}. Other metal ions, however, are bound but not reduced, e.g., K^{+}. The source of electrons for selective metal ion reduction has been speculated to be water but never empirically shown. Here, using $H_2{}^{18}O$, we show that when MB from *Methylocystis sp*. strain SB2 (MB-SB2) and *Methylosinus trichosporium* OB3b (MB-OB3) were incubated in the presence of either Au^{3+}, Cu^{2} , and Ag^{+}, $^{18,18}O_2$ and free protons were released. No $^{18,18}O_2$ production was observed either in presence of MB-SB2 or MB-OB3b alone, gold alone, copper alone, silver alone or when K^{+} or Mo^{2+} was incubated with MB-SB2.

In contrast to MB-OB3b, MB-SB2 binds Fe^{3+} with an N_2S_2 coordination and will also reduce Fe^{3+} to Fe^{2+}. Iron reduction was also found to be coupled to oxidation of $2H_2O$ and generation of O_2. MB-SB2 will also couple Hg^{2+}, Ni^{2+} and Co^{2+} reduction to the oxidation of $2H_2O$ and generation of O_2, but MB-OB3b will not, ostensibly as MB-OB3b binds but does not reduce these metal ions.

To determine if the O_2 generated during metal ion reduction by MB could be coupled to methane oxidation, $^{13}CH_4$ oxidation by *Methylosinus trichosporium* OB3b was monitored under anoxic conditions. The results demonstrate O_2 generation from metal ion reduction by MB-OB3b can support methane oxidation.

IMPORTANCE

The discovery that MB will couple the oxidation of H_2O to metal ion reduction and the release of O_2 suggests that methanotrophs expressing MB may be able to maintain their activity in hypoxic/anoxic conditions through "self-generation" of dioxygen required for the initial oxidation of methane to methanol. Such an ability may be an important factor in enabling methanotrophs to not only colonize the oxic-anoxic interface where methane concentrations are highest, but also tolerate significant temporal fluctuations of this interface. Given that genomic surveys often show evidence of aerobic methanotrophs within anoxic zones, the ability to express MB (and thereby generate dioxygen) may be an important parameter in facilitating their ability to remove methane, a potent greenhouse gas, before it enters the atmosphere.

INTRODUCTION

Aerobic methane oxidizing bacteria (methanotrophs) oxidize methane to carbon dioxide via a series of two electron steps with methanol, formaldehyde and formate as intermediates (1). The initial oxidation of methane to methanol is an oxygen and energy dependent reaction and is catalyzed by either a soluble cytoplasmic methane monooxygenase (sMMO) or a particulate or membrane-associated methane monooxygenase (pMMO) (1-8). The reductant for the initial oxidation of methane is supplied by NADH for the sMMO and by quinols for the pMMO (2, 3, 9-11). Methanol is oxidized to formaldehyde by a calcium or rare earth dependent methanol dehydrogenase using a *c*-type cytochrome as an electron acceptor (12-17) Formaldehyde is either assimilated or oxidized using either NAD^+ or quinone as the electron acceptor (10, 18-

20). The final two electron oxidation of formate to carbon dioxide is catalyzed by the NAD^+-linked formate dehydrogenase (21-23). Electrons from NADH, quinol or cytochrome *c* are either utilized in biosynthetic reactions or oxidized for energy using either dioxygen (11), nitrate (24) or ferric iron (25) as the terminal electron acceptor.

In methanotrophs capable of expressing both forms of the MMO, expression is regulated by copper (1, 9, 26-28). In addition to the MMOs, a number of genes are regulated by copper (1) and some methanotrophs of the *Alphaproteobacteria* have a novel copper acquisition systems based on the extracellular copper binding peptide methanobactin (MB) (29-31). Methanobactins (MBs) are low molecular mass (<1,300Da), high potential (E_m 483 – 745 mV) ribosomally synthesized post-translationally modified peptides (RiPPs) and were the first examples of a chalkophore, i.e., a compound excreted by bacteria for the purpose of scavenging copper from the surrounding environment (30, 32). Structurally MBs are divided into two groups. Both Group I and II MBs are characterized by an internal oxazolone group with an associated thioamide and a second N-terminal 5 or 6 membered ring which in Group I MBs is either an oxazolone or pyrazinedione group with an associated thioamide while Group II MBs has either an imidazoline or pyrazinedione group with an associated thioamide (30, 32-36). The ring and associated thioamide are derived from an X-Cys dipeptide via a series of partially characterized post-translational modifications (29, 31, 37). Group I MBs are characterized by an internal disulfide bridge and the copper bound form a dicyclic structure (33, 34, 38). Group II MBs lack this disulfide bridge and the copper bound form has a hairpin-like structure and is characterized by a central sulfonated threonine (30, 36).

In addition to copper ions, MBs will bind many metal ions (39-42) and reduce some, but not all metal ions that are bound (39, 43). In MB from *Methylosinus trichosporium* OB3b, MB-OB3b, metal ions such as copper, silver and gold are coordinated via an N_2S_2 ligand set utilizing a N from each ring and the two thioamides and these metals are reduced after binding (30, 34, 39, 44). Other metal ions such as iron, nickel and cobalt are coordinated via an N_1S_1 ligand set using one ring and its associated thioamide and are not reduced (39). Based on coordination metals were classified as either Group A metals coordinated by a N_2S_2 ligand set, or Group B metals coordinated by a N_1S_1 ligand set. In contrast, all of the metals bound by MB from *Methylocystis* strain SB2 (MB-SB2) are coordinated by a N_2S_2 ligand set ((40, 41, 43, 45) and this report).

Since metal ion reduction assays are often carried out in unbuffered reaction mixtures in the absence of an external reductant, water has been proposed, but not shown to be the electron donor (36). Here, we examine the binding and reduction of oxidized forms of gold (as $HAuCl_4$), copper (as $CuCl_2$), silver (as AgF), iron (as $FeCl_3$), nickel (as $NiCl_2$), mercury ($HgCl_2$), cobalt (as $CoCl_2$) and potassium (as KCl) in the presence and absence of $H_2{}^{18}O$ by MB-SB2 as well as the binding and reduction of gold, copper and silver in the presence of $H_2{}^{18}O$ by MB-OB3b.

RESULTS

Spectral and Thermodynamic Properties of $AuCl_4^-$ binding by MB-SB2

UV-visible absorption, fluorescence and circular dichroism spectra (Figs. S1-S3) and thermodynamic measurements (Fig. S4; Table S1) demonstrate changes following the addition

of $HAuCl_4$ to MB-SB2 were complex with transitions apparent at 0.25, 0.5, 0.75, 1.0 and 2.0 Au per MB-SB2. As MB-SB2 has only one identified metal binding motif (i.e. an N_2S_2 ligand set), we therefore interpret these data to indicate changes in Au coordination, when MB-SB2 transitions from an oligomeric state(s) to a monomer.

The increased fluorescence emission intensity following $HAuCl_4$ addition may be due to disruption of internal quenching between the imidazolone and oxazolone groups and is consistent with the intramolecular exciton transfer previously demonstrated following hydrolysis of the oxazolone group (43)(Fig. S2). The decreased fluorescence at $HAuCl_4$ to MB-SB2 ratios greater than 1.0 suggests direct metal quenching or intra-/ inter-exciton transfer between the oxazolone and imidazolone groups, or may be associated with nanoparticle formation which occurs at Au to MB-SB2 ratios greater than 1:1.

As Au nanoparticle formation requires Au^{3+} reduction (46), nanoparticle formation (Fig. S5; Table 2S) by MB-SB2 indicated that MB-SB2 binds and reduces multiple Au^{3+} to Au^0. Such findings accentuated the need to determine the electron source for metal reduction by MBs. To extend these preliminary studies, we examined reduction of $HAuCl_4$ via MB-SB2 when dissolved in either $H_2{}^{16}O$ or $H_2{}^{18}O$.

X-Ray Photoelectric Spectroscopy (XPS), Kinetics and Chloride Determination

In reaction mixtures containing $HAuCl_4$ and MB-SB2 dissolved in $H_2{}^{16}O$, MB-SB2 was observed to reduce $AuCl_4^-$ to $Au^0 + 4Cl^-$, as determined by XPS and argentometric titrations, respectively (Fig. 1; Table 1). MB-SB2 reduced up to 19 Au^{3+} to 19Au^0 with a time-dependent average Au^{3+} to Au^0 reduction rate of 0.3 ± 0.06 min^{-1} for those assays where rates could be determined. This time-

dependent reduction was the reason samples were frozen in liquid nitrogen and lyophilized overnight to stop the reaction and dry the samples for analysis. As observed with MB-OB3b (39), Au^{3+} and Au^{0} were the only oxidation states detected, indicating a direct three-electron reduction of $HAuCl_4$ (Fig. 1).

Kinetics of $AuCl_4^-$ Binding and Reduction

The time course for the binding of Au^{3+} to the oxazolone and imidazolone rings in MB-SB2 was measured as the decrease in absorbance at 341 and 389 nm, respectively, following stopped-flow mixing of MB-SB2 with Au^{3+} at 4°C (Fig. 2A). Unfortunately, even at 4°C, initial binding rates could only be determined for the oxazolone ring, since the binding to the imidazolone ring was complete before mixing of the sample was complete (1.4 msec). In contrast, the binding rates to the oxazolone ring were low, 12 - 57 s^{-1}, at $Au^{3+}$to MB-SB2 ratios below 0.3, increased at Au^{3+} to MB--SB2 ratios between 0.3 and 1.5 Au^{3+} per MB-SB2 up to a maximum rate of ~1600 s^{-1}, followed by a decline in rate at molar ratios >1.5 Au^{3+} per MB-SB2 (Fig. 2A).

Au^{3+} reduction rates (0.3 ± 0.06 min^{-1}; Table 1) were much slower to the initial binding rates (greater than 2,000 s^{-1}; Fig. 2A). The difference may be due to the different binding rates between the imidazolone and oxazolone groups. Monitoring the florescent changes over time at $HAuCl_4$ to MB-SB2 below 1:1, suggest final Au coordination required several minutes to complete (Fig. 2B). At gold to MB-SB2 concentrations greater than 1.0 an initial disruption of exciton coupling resulting in increased florescent intensity followed by quenching (Fig. 2B). What is pertinent to this discussion is that Au initially binds primarily if not exclusively to the

155 imidazolone group followed by binding to the oxazolone group and a final reorientation. The
156 time scale for these changes are in keeping with gold reduction rates.
157
158 **Oxidation of H_2O coupled to Au^{3+} reduction by MB-SB2**
159 As four Cl^- were generated in reaction mixtures for every $HAuCl_4$ reduced to Au^0, chlorine was
160 ruled out as a potential electron donor. To determine if H_2O was the electron donor, H^+
161 concentrations were monitored during $HAuCl_4$ titrations of MB-SB2. Unfortunately, pH changes
162 associated with the addition of $HAuCl_4$ to unbuffered reaction mixtures made pH changes
163 associated with binding of $AuCl_4^-$ difficult to determine (Fig. 3A). To examine if H_2O could serve
164 as an electron source for Au^{3+} reduction, $^{18,18}O_2$ production was monitored in reaction mixtures
165 containing 97% $H_2{}^{18}O$. No $^{18,18}O_2$ production was observed in reaction mixtures containing
166 either MB-SB2 alone (Fig. 4A) or $HAuCl_4$ alone (result not shown). However, following $HAuCl_4$
167 addition to MB-SB2, $^{18,18}O_2$ was observed demonstrating the coupling of water oxidation with
168 metal reduction (Figs. 4B and 5).
169 It should be noted that there is seemingly an electron imbalance, with three electrons
170 required for Au^{3+} to Au^0 while four electrons are released for every two molecules of water
171 oxidized. There are two possibilities to resolve this issue (47) the reduction of four atoms of
172 Au^{3+} are coupled to the oxidation of six molecules of water and (2) the reduction of one atom of
173 Au^{3+} is coupled to the oxidation of two molecules of water with the fourth electron used to
174 reduce dioxygen to superoxide. Assays show that reduced MB-SB2 will reduce dioxygen to
175 superoxide (Table S3). Under the low pH conditions following $HAuCl_4$ addition to MB-SB2 (Fig.
176 3) superoxide would be expected to undergo dismutation reactions generating H_2O_2 (48). In

addition, as observed in MB-OB3b (49), Au-MB-SB2 complexes show superoxide dismutase activity (Table S3). Thus, H_2O_2 should appear in reaction mixtures if the fourth electron was used to reduce dioxygen. The rate of $^{18,18}O_2$ production increased by approximately 18% following the addition of catalase, suggesting the production of H_2O_2 (Fig. 5).

Oxidation of H_2O coupled to Cu^{2+} reduction by MB-SB2

Although the oxidation of water to dioxygen coupled to Au^{3+} reduction is chemically interesting it is not likely biologically relevant. To determine if the oxidation of H_2O was specific to Au^{3+} reduction or a more general property of metal ion reduction by MB-SB2, similar experiments in $H_2{}^{18}O$ were carried out with $CuCl_2$ as it is believed the primary purpose of MB is the collection of copper critical for methanotrophic activity. Previous spectral and thermodynamic studies have shown MB-SB2 will reduce multiple Cu^{2+} to Cu^{+} in the absence of an external reductant, suggesting that water served as the reductant (43). $^{18,18}O_2$ evolution was observed following the addition of $CuCl_2$ to a $H_2{}^{18}O$ solution of MB-SB2 (Fig 4C). Further, such evolution followed a similar trend to that for $HAuCl_4$ and a substantial pH drop was observed (Fig. 3B - 5). Perhaps of greater environmental relevance is the finding of substantial (>100 µM) evolution of dioxygen from water oxidation when MB-SB2 bound and reduced copper (Fig. 5).

The ratio of $AuCl_4^-$ and Cu^{2+} to MB-SB2 in the experiments described above, as well as other metals showing $^{18,18}O_2$ production (Fig. 4) described below was 10:1. To determine the number of electrons needed to be extracted from MB-SB2 before water oxidation occurs, reaction mixtures containing 0.5, 1, 2, 3, 4, and 5 Cu^{2+}per MB-SB2 in 97% $H_2{}^{18}O$ were examined. No $^{18,18}O_2$ was observed in samples containing 0.5, 1, 2, 3, or 4 Cu^{2+} per MB-SB2 (results not

shown). $^{18,18}O_2$ was observed in samples containing 5 Cu^{2+} per MB-SB2 indicating for the initial water oxidation to occur five electrons must be extracted from MB-SB2 (Fig.4D).

K^+ was also examined as a metal ion bound by MB-SB2 (Fig. S6A), but not reduced, as no evidence of the formation of metallic K^0 was observed (50). No $^{18,18}O_2$ was observed following the addition of KCl (Fig.4E) and comparatively minor changes in pH (Fig. 3C) were observed demonstrating water oxidation by MB-SB2 after binding a metal ion is contingent upon that metal being reduced. MB-SB2 does not bind Mo^{2+} (Fig. S6B) and was used as a negative control. As expected, no $^{18,18}O_2$ was observed in reaction mixtures containing $NaMoO_4$ and MB-SB2 (results not shown).

Oxidation of H_2O coupled to Ag^+, Hg^{2+} Fe^3, Ni^{2+} and Co^{2+} reduction by MB-SB2

As described above Group A metal ions bound by MB-OB3b are reduced following binding. Ag^+ and Hg^{2+} are Group A metals, MB-SB2 bound both metals via an N_2S_2 coordination (Figs. S6C and S6D) and $^{18,18}O_2$ was observed in reaction mixtures containing MB-SB2 and AgF (Fig. 4F) or $HgCl_2$ (Fig. 4G) at levels similar to that observed with gold and copper .

In contrast to MB-OB3b (39), MB-SB2 binds all metal ions tested via an N_2S_2 coordination (40, 41, 43) (Fig. S6). Also in contrast to MB-OB3b, MB-SB2 will reduce Fe^{3+} to Fe^{2+} at a rate of 1.02 ± 0.09 min^{-1} as measured via the ferrozine assay (51, 52)(Fig. 6A). In fact, MB-SB2 will dissolve insoluble Fe^{3+} hydroxides in the light (Fig. S6E insert) or dark (Fig. 6C). The one electron ferric iron reduction rate was approximately three times faster than the three electron gold reduction rate. In reaction mixtures containing MB-SB2 and $FeCl_3$ (Fig. 4H) $^{18,18}O_2$ was observed at concentrations 1.3 ± 0.1 fold higher than those observed with Au^{3+} and Cu^{2+}.

221 $^{18,18}O_2$ was also observed in reaction mixtures containing $NiCl_2$ (Figs. 4I and S6F) or $CoCl_2$ (Figs.
222 4H and S6G) and MB-SB2, although the concentration of $^{18,18}O_2$ was consistently low with $CoCl_2$.
223

224 **Oxidation of H_2O coupled to Au^{3+}, Cu^{2+}, and Ag^+ reduction by MB-OB3b**

225 To determine if water oxidation coupled to metal ion reduction was specific to MB-SB2, a
226 Group II MB, or a more general property of MBs, water oxidation was examined in the Group I
227 MB from *M. trichosporium* OB3b (MB-OB3b) (53). Previous studies have shown MB-OB3b binds
228 and reduces Au^{3+}, Cu^{2+} and Ag^+ to Au^0, Cu^+ and Ag^0, respectively, and bound but did not reduce
229 Fe^{3+} (Fig. 6B; (39, 44)). Thus, $^{18,18}O_2$ production was monitored in reaction mixtures containing
230 $HAuCl_4$, $CuCl_2$, AgF and $FeCl_3$ with or without MB-OB3b prepared in 97% $H_2{}^{18}O$. Again, no $^{18,18}O_2$
231 production was observed in reaction mixtures containing either MB-OB3b alone (Fig. 7A) or
232 with $HAuCl_4$, $CuCl_2$ or AgF alone (result not shown). However, following $HAuCl_4$ (Fig. 7B), $CuCl_2$
233 (Fig. 7C) or AgF (Fig. 7D) addition to reaction mixtures containing MB-OB3b, $^{18,18}O_2$ was
234 observed although the concentrations of $^{18,18}O_2$ were less than 25% of the $^{18,18}O_2$ produced in
235 similar reactions with MB-SB2. No $^{18,18}O_2$ was observed following $FeCl_3$ addition to a reaction
236 mixture containing MB-OB3b.
237

238 **Methane oxidation coupled to O_2 generated from Cu^{2+} reduction by MB-OB3b**

239 To determine if dioxygen generated during metal ion reduction could support methane
240 oxidation by *M. trichosporium* OB3b, incubations with $^{13}CH_4$ in the presence and absence of
241 MB-OB3b and Cu^{2+} were performed under anoxic conditions in an anaerobic glove box. In cell
242 suspensions with no additional amendments of either copper or MB-OB3b, 0.72 $\pm$ 0.17 µmol

243 $^{13}CO_2$ was observed after three days (assumed to be driven by the presence of residual
244 dioxygen in the reaction mixtures (Fig. 8)). In cell suspensions amended with 25 µM Cu^{2+}, 0.97 ±
245 0.03 µmol $^{13}CO_2$ was observed (a 34% increase, not significantly different from the amount of
246 $^{13}CO_2$ measured with no amendment, p = 0.06). If 5 µM MB-OB3b were added instead, 1.47 ±
247 0.08 µmol $^{13}CO_2$ was measured (an increase of ~104%, significantly greater from no
248 amendment, p = 2.2 x 10^{-3}, presumably to MB-OB3b binding and reducing metals part of the
249 growth medium). If both 25 µM Cu and 5 µM MB-OB3b were added, 2.5 ± 0.37 µmol $^{13}CO_2$ was
250 observed, an increase of ~250% from that in no amendment (again significantly different, p =
251 1.5 x 10^{-3}), indicating that metal ion reduction by MB can support methane oxidation in anoxic
252 conditions (Fig.8).
253

254 **DISCUSSION**

255 Metal ion binding by MBs has focused on MB-OB3b, a Group I MB (34, 39, 44). MB-OB3b
256 bound Group A metal ions such as Cu^{2+}, Au^{3+}, Ag^{+}, Hg^{2+} via an N_2S_2 ligand set. Other metal ions
257 such as Fe^{3+}, Co^{2+}, Cd^{2+} Mn^{2+}, Ni^{2+} and Zn^{2+} showed an N_1S_1 coordination and were placed in
258 Group B. Of the metal ions examined Group A metals were reduced following binding whereas
259 Group B metal ions were not. In this and previous reports (40, 41, 43, 45), MB-SB2, a Group II
260 MB, coordinates all metals bound via N_2S_2 coordination and reduced metals previously place
261 Group A and B. With the exception of K^{+}, metal ions bound via an N_2S_2 coordination are
262 reduced and here we show that H_2O can serve as an electron donor driving metal ion reduction.
263 The finding that MB, after binding specific metal ions can split water to form dioxygen
264 and that this reaction can drive methane oxidation under anoxic conditions suggests that this

may be another strategy whereby aerobic methanotrophy can occur in an anoxic environment. That is, it has been shown that methane oxidation via aerobic methanotrophy occurs in anoxic zones of shallow lakes (i.e., at a depth of ~10 m), with such activity driven by oxygenic photosynthesis as sunlight could penetrate to this depth (54, 55). In these studies, it was found that methane oxidation rates increased in the light vs. dark, and such activity was abolished when a selective inhibitor of photosynthesis was added. Thus, it appears that methanotrophs can form very effective relationships with oxygenic photosynthetic microbes to scavenge trace amounts of dioxygen, and by so doing, enhance methane removal from these environments.

More germane to the findings here, however, is the discovery that aerobic methanotrophs were also active in deep lake water (~160 m) where oxygenic photosynthesis is highly unlikely as sunlight cannot penetrate to this depth (56). Such activity, however, could be stimulated by the addition of dioxygen and oxidized metals. Here it was concluded that methanotrophs may survive anoxic environments by utilizing alternative electron acceptors. Others have shown that aerobic methanotrophs of the *Methylobacter* genus can be stimulated in anoxic lake waters through the addition of either nitrate or sulfate (57). Indeed, it has been shown that some aerobic methanotrophs can respire nitrate (24) or ferric iron (25). Such a strategy could conserve trace amounts of dioxygen to enable methane oxidation by the MMOs. Alternatively, it has been shown that some methanotrophs will couple methane oxidation to fermentation to putatively conserve dioxygen (58), and such a strategy has been speculated to be responsible for methanotrophic activity in dioxygen-limited lakes (57). Finally, it has been speculated that alternatively or in conjunction, methanotrophs may form syntrophic partnerships with other microbes to facilitate methane oxidation (57) when dioxygen is limiting.

It should be noted, however, that in studies of methane oxidation in anoxic lake water samples, great care was taken to exclude any oxygen intrusion and any trace amounts of oxygen present were quite small and could not explain the extent of methane oxidation observed. How these microbes then are able to oxidize methane in the absence of dioxygen is still unclear. That is, for the identified methanotrophs to oxidize methane, dioxygen is required for either form of MMO regardless if alternative terminal electron acceptors can be used or if effective microbial partnership(s) can be formed. Thus, either unknown sources of dioxygen exist in these environments and/or these microbes possess some novel, as yet undescribed mechanism of anaerobic methane oxidation, i.e., novel forms of MMO that can utilize oxidized sulfur and nitrogen species in place of dioxygen.

Here we present an alternative explanation for the presence and activity of aerobic methanotrophs in anoxic environments, particularly alphaproteobacterial methanotrophs. That is, genes for MB biosynthesis have only been found in the genomes of various *Methylosinus* and *Methylocystis* species of the *Alphaproteobacteria* (53). It has been repeatedly shown that these genera prefer high methane/low oxygen conditions found at the oxic-anoxic interface *in situ* (59, 60). Further, they are the predominant methanotrophic genera present in completely anoxic zones of rice paddy soils (61). Thus, it is tempting to speculate that the ability to produce MB enables methanotrophs to colonize methane-rich environments by self-producing dioxygen to ensure that methane oxidation can continue even when ambient concentrations of dioxygen are quite low. Such a strategy is particularly important for methanotrophs that colonize the oxic-anoxic interface in soils, for not only are these locations dark (thus excluding the possibility of methanotrophy/phototrophy synergy), this interface shifts quickly in response to episodic

precipitation and drying periods. As such, methanotrophs that colonize this interface must be prepared to tolerate periodic and possibly quite extended anoxic conditions. The ability to produce dioxygen from water would thus enable these microbes to continue to oxidize methane under anoxia, thereby generating ATP, as well as providing intermediates required for carbon assimilation (i.e., formaldehyde). Doing so would enable them to survive extended periods in the absence of oxygen, if not allow for some continued growth in anoxic conditions.

It should be noted, however, is that in aforementioned lake studies concluding aerobic methanotrophy occurs in anoxic environments, gammaproteobacterial methanotrophs appeared to be predominantly responsible for methane oxidation and to date, no representatives of this group have been shown to have the genes required for MB biosynthesis, although it is clear that at least some can and do secrete a copper-binding compound (62). It may be that these methanotrophs utilize dioxygen created by others via MB production (i.e., some sort of collaboration between gamma- and alpha-proteobacteria as concluded between methanotrophs and oxygenic photosynthetic microbes) and/or also can generate dioxygen via some unknown mechanism.

Finally, prior to discovery of dioxygen production via splitting of water by metal-MB complexes reported here, dioxygen production by biological systems has been observed in only four known pathways: oxygenic photosynthesis (63, 64), detoxification of oxygen radicals (65, 66), (per)chlorate respiration (67) and nitric oxide dismutation by *Candidatus* Methylomirabilis oxyferans of the NC10 phylum (68). The latter two mechanisms may provide some explanation as to the significance of MB-mediated water oxidation. That is, it has been shown that dioxygen evolution from (per)chlorate respiration occurs when the intermediate chlorite is dismutated to

chloride and dioxygen, and it is speculated that the dioxygen is then used for an antibiotic-producing monooxygenase in *Haloferaxvol- volcanii* (69). Further, *Ca*. M. oxyferans is a methanotroph, but respires nitrite rather than dioxygen. Interestingly, dioxygen is critical for its growth as this microbe utilizes the membrane-associated methane monooxygenase for methane oxidation to methanol (68). Stable isotope studies showed that *Ca*. M. oxyferans dismutates nitric oxide to dinitrogen and dioxygen, the latter which is used for methane oxidation (the mechanism(s) by which this occurs, however, is still unknown). It may be that MB-expressing aerobic methanotrophs perform a similar feat to ensure that there is adequate dioxygen for continued MMO activity in hypoxic/anoxic conditions.

In conclusion, the discovery of water oxidation by specific metal-methanobactin complexes is not only unusual, it also implies a strategy whereby aerobic methanotrophs can survive, if not thrive in anoxic conditions. As such, MB-driven dioxygen generation may be an important but hitherto unrecognized process whereby methane emissions are regulated.

MATERIALS AND METHODS

Materials

Anhydrous $CuCl_2$ (Acros Organics, Geel, Belgium), $HAuCl_4$ (Acros Organics), $HgCl_2$ (Acros Organics, Geel, Belgium), AgF (Acros Organics, Geel, Belgium), $FeCl_3$ (Acros Organics, Geel, Belgium), $NiCl_2$ (Acros Organics, Geel, Belgium), $CoCl_2$ (Acros Organics, Geel, Belgium), $NaMoO_4$ (Sigmal-Aldrich) and KCl (Sigmal-Aldrich) were stored in a desiccator under Ar_2. $H_2{}^{18}O$ was obtained from Cambridge Isotope Laboratories, Inc. (Andover, MA, USA) and $^{18,18}O_2$ from Sigma Aldrich. Ar_2, $^{16,16}O_2$ and CP grade CH_4 were obtained from Airgas USA LLC. HPLC grade

353 acetonitrile, methanol and other reagents/chemicals were purchased from Fisher Scientific and
354 used without additional purification. Dianion HP-20 was purchased from Sigma-Aldrich C. LLC.
355

356 **Organism, Culture Conditions and Isolation of Methanobactin**

357 *Methylocystis* strain SB2 and *M. trichosporium* OB3b were cultured in nitrate mineral salts
358 media (70) amended with either 0.2 or 1.0 µM $CuSO_4$ to optimize production of its
359 methanobactin (MB-SB2). MB-SB2 was purified from the spent media as previously described
360 with the following exception (71). The freeze-dried sample from the Dianion HP20 column was
361 resuspended in deionized H_2O and loaded onto a 250mm x 20mmTarga C18 column (Higgins
362 Analytical Inc., Mountain View, Ca, USA) on an Azurk HPLC system (Knauer, Berlin, Germany).
363 MB-SB2 eluted in the 12-25% methanol fraction in a methanol:H_2O gradient. The purified
364 methanobactin was then freeze-dried as described above.
365

366 **X-Ray Photoelectric Spectroscopy (XPS)**

367 XPS was performed as previously described (39, 44) with the following modifications. $HAuCl_4$
368 and $HAuCl_4$ plus MB-SB2 samples were dried onto highly oriented pyrolytic graphite by freeze-
369 drying. The 1 cm square graphite substrates were immersed in either $HAuCl_4$ or $HAuCl_4$ plus MB-
370 SB2 solutions, frozen in liquid nitrogen and lyophilized overnight. The graphite was then
371 mounted onto an XPS puck and analyzed. Other drying methods were employed such as drying
372 in air under a stream of He gas with a drying time of 30 min or filtered through a porous
373 alumina filter followed by a 2 min drying time. However, samples produced by these methods
374 showed additional reduction.

375 As previously observed (39), XPS analysis of Au was complicated by X-ray induced
376 reduction during the measurement process. Au 4f peak areas were therefore measured as a
377 function of X-ray exposure, the peak areas for a given X-ray dose determined using the CASA
378 XPS fitting program, and the areas plotted as a function of time. An exponential fit to the data
379 using Igor Pro fitting program allowed a determination of the unirradiated sample's Au^{3+} and
380 Au^{0} peak areas.

381 XPS measurements were carried out on a custom-designed system that incorporated a
382 SPECS hemispherical analyzer (SPECS Scientific Instruments, Sarasota, FL, USA), Al X-ray source,
383 and load-lock to allow for rapid sample exchanges.

384

385 **Kinetics of Au^{3+} Binding.** The rates of Au^{3+} binding to mb-SB2 were determined by measuring
386 absorption changes at 338 nm and 387 nm using a four-syringe Biologic SFM/4000/S stopped
387 flow reactor coupled to a MOS-500 spectrophotometer (Bio-Logic (40). Science Instrument SA,
388 Claix, France) at 4°C as previous described (40). In contrast to the absorbance maxima using
389 Cary 50 spectrometer, the absorbance maximum for the oxazolone was 338 nm and for the
390 imidazolone ring 387 nm on with this system. Stock solutions of $HAuCl_4$ were prepared in
391 >18MΩ▪cm H_2O. The stock solutions for MB-SB2 were prepared by dissolving freeze-dried MB-
392 SB2 in > 18MΩ▪cm H_2O. Final concentration of the stock solutions of MB-SB2 were determined
393 after filtration by UV-visible absorption spectroscopy as previously described (40). Path length
394 for the cuvette used in the Biologic SFM/4000/S stopped flow reactor was 1.5 mm and dead
395 time of the system was 1.4 ms. The system was cooled and maintained at 4°C. Reaction
396 mixtures contained 400 µM of MB-SB2 and either 40, 100, 200, 240, 280, 320, 360, 400, 600,

700, or 800 µM of $HAuCl_4$. Rates obtained for each concentration were an average of either 5 or 7 traces. The rates were determined by fitting the traces to the exponential function in Biokine operational software (Bio-Logic Science Instrument SA). Binding rates were calculated in mol Au bound per sec per mol MB-SB2 and reported as the binding number (s^{-1}).

Fluorescence changes overtime were monitored at 429 nm on a Cary Eclipse (Agilent Technologies Inc. Santa Clara, CA, USA following excitation at 341nm.

Water Oxidation

Saturated solutions of anhydrous $CuCl_2$, $HAuCl_4$, $HgCl_2$, AgF, $FeCl_3$, $NiCl_2$, $CoCl_2$, $NaMoO_4$ and KCl were prepared in a Coy anaerobic chamber (atmosphere 95% Ar 5% H_2)(Coy Laboratory Products, Ann Arbor, MI, USA). Oxidation of $2H_2O$ to $O_2 + 4H^+$ in reaction mixtures containing a metal ion and either MB-SB2 or MB-OB3b was determined by monitoring production of $^{18,18}O_2$ and H^+ and in the case of $HAuCl_4$, production of Cl^-. In oxygen evolution experiments, freeze-dried MB-SB2, MB-OB3b, catalase, as well as anhydrous metal stock solution were prepared in 97% $H_2{}^{18}O$ (Sigma Aldrich, St. Louis, Mo, USA) in 0.8 ml brown airtight vials (DWK Life Sciences, Millville, NJ, USA). Reaction mixtures contained 0 or 2mM MB-SB2 or MB-OB3b and 0 – 20mM metal ion in a final volume of 100µl $H_2{}^{18}O$. Reaction mixtures were prepared in 2 ml brown serum vials, sealed with Teflon lined silicon septa. Initial experiments were determined with aluminum foil wrapped vials, but that practice was discontinued once it was clear that identical results were produced regardless if vials were wrapped or not. Generation of $^{18,18}O_2$ from $H_2{}^{18}O$ was monitored by direct injection (1µl or 2µl) of head space.

418 Gas samples were manually injected into an Agilent 7890B GC system (Santa Clara, CA,
419 USA with a 7250 Accurate-Mass Q-TOF GC/MS and a DB5-ms column. Except for the $^{18,18}O_2$
420 injections for standard curves, all injections were 1µl using gas tight Hamilton syringes.
421 Standard curves were generated with 1µl, 1.5µL and 2 µl injections of 97% $^{18,18}O_2$ (Sigma
422 Aldrich, St. Louis, Mo, USA). The head space in the vials was sampled before and after the
423 addition of the metals, as was the outside air in the mass spectroscopy as controls. After the
424 standards and controls were injected, the samples were mixed and head space samples were
425 immediately collected, with subsequent samples taken every 30-60 seconds. After several
426 minutes, collection slowed to 1 sample every 2-3 minutes. The quantization of generated $^{18,18}O_2$
427 came from an extracted-ion chromatogram set to 35.9978 Da. A small shift in the MS location
428 of the $^{18,18}O_2$ was observed on some dates. If a drift in the MS of $^{18,18}O_2$ was observed, identity
429 of the peak was verified with 97% $^{18,18}O_2$ standard.
430
431 **Oxidase, Superoxide Dismutase, Hydrogen Peroxide Reductase and Iron reductase Activity**
432 **and pH Measurements**
433 Oxidase, superoxide dismutase and hydrogen peroxide reductase activity were determined as
434 previously described by Choi *et al*. (49). Ferrozine assay was used to determine iron reductase
435 activity (51, 52).
436 pH changes during metal titrations were monitored on either a Radiometer PHM 220
437 meter with a pH2005-7 combined pH electrode (Radiometer Analytical, Villeurbanne Cerdex,
438 France) or on an Oakion Ion 700 pH meter (Cole-Parmer, Vermon Hills, IL, USA).

439 Free chloride produced from the binding and deduction of $HAuCl_4$ to Au^0 was measured
440 via argentometric titration (72). $HAuCl_4$:MB-SB2 solutions were prepared at a molar ratio of 9:1
441 and incubated for at least 72 h. Following the incubation period, the solution was titrated with
442 a standardized $AgNO_3$ solution, delivered with a Ramé-hart 2.0 ml microsyringe. The titration
443 processes were monitored with a custom-made Ag wire working electrode and Ag/AgCl
444 reference electrode.
445
446 **Methane oxidation coupled to O_2 generated from Cu^{2+} reduction by MB-OB3b**
447 **Sample preparation.** *M. trichosporium* OB3b was grown on nitrate mineral salts medium (NMS)
448 (70) at 30°C in 250-ml side-arm flask sealed with rubber stoppers. Cultures were shaken at 200
449 rpm under a methane-to-air ratio of 1:2, until the mid-exponential phase (OD_{600} ~ 0.3). 2 ml of
450 the cell culture was then transferred to 8.5 ml serum vials containing a Teflon-coated magnetic
451 stir bar. Four separate conditions were prepared: (1) *M. trichosporium* OB3b with no
452 amendments; (2) *M. trichosporium* OB3b + 25 µM copper (5 µl added from a filter sterilized
453 (0.22 µm) 10 mM stock solution of $CuCl_2$); (3) *M. trichosporium* OB3b + 5 µM MB-OB3b (10 µl
454 added from a filter sterilized (0.22 µm) 1 mM stock solution of MB-OB3b), and (4) *M.*
455 *trichosporium* OB3b + 25 µM copper + 5 µM MB-OB3b. Biological triplicate samples were
456 prepared for all conditions. The vials were then crimp-sealed and degassed using pre-purified
457 grade filter-sterilized (0.22 µm) nitrogen gas (N_2, 99.998%) for 20 minutes at a flow rate of 3.42
458 ml/s using 22- and 25-gauge needles for N_2 gas flow in and out. After degassing, the needles
459 were removed and the samples immediately placed in an anaerobic chamber filled with a H_2/N_2
460 gas mixture (1:9 mixing ratio). Once in the anaerobic chamber, 1 ml of ^{13}C-labeled methane

($^{13}CH_4$, 99%) (Sigma-Aldrich, St. Louis, MO) was added using a 10 ml gas-tight syringe (Hamilton Company, Reno, NV). Vacuum-grease was then spread on the top of the sealed septa. The vials were finally covered by aluminum foil and incubated inverted (septum side down) on a magnetic stir plate in the anaerobic chamber for 3 days at 25°C.

Gas chromatography/mass spectrometry analysis. Gas chromatography/mass spectrometry (GC/MS) analyses was performed using an Agilent 7890B gas chromatograph system coupled with Agilent 5977B single quadrupole mass spectrometer (Agilent Technologies, Santa Clara, CA, USA). A Carboxen®-1010 PLOT capillary column with 30 m × 0.32 mm was used for separation (Supelco, Bellefonte, PA). 10 µL of headspace gas of each sample was injected manually using a 25 µL gas-tight syringe (Hamilton Company, Reno, NV). GC system conditions were as follows: carrier gas and flow rate, He 10 ml/min; split injection with split ratio of 5:1; inlet temperature 170°C; oven temperature maintained at 145°C throughout the analysis. The mass spectrometry ion source and quadrupole temperatures were 250°C and 200°C, respectively. Under these conditions $^{13}CH_4$ and $^{13}CO_2$ were detected at 2.16 min and 2.86 min, respectively. Data were acquired in selected ion monitoring (SIM) mode, monitoring *m/z* 17 for $^{13}CH_4$ and *m/z* 45 for $^{13}CO_2$.

ACKNOWLEDGEMENTS

Funding: This research was supported by the U.S. Department of Energy Office of Science (Grants #DE-SC0018059; JDS and ADS), the National Science Foundation (Grant #1912482; JDS), the Materials Science and Engineering Center at UW-Eau Claire (MTM), and the ISU Bailey Research and Career Development (TAB). Use of ITC and Biologic SFM/4000 stopped flow

483 reactor coupled to a MOS-500 spectrophotometer was made possible through a generous gift

484 from the Roy J. Carver Charitable Trust (Muscatine, Iowa).

485 **Competing interests:** Authors declare they have no competing interests.

486 **REFERENCES**

487 1. Semrau JD, DiSpirito AA, Yoon S. 2010. Methanotrophs and copper. FEMS Microbiol
488 Rev 34:496-531.

489 2. Basu P, Katterle B, Andersson KK, Dalton H. 2003. The membrane-associated form of
490 methane mono-oxygenase from *Methylococcus capsulatus* (Bath) is a copper/iron
491 protein. Biochem J 369:417-427.

492 3. Choi DW, Kunz RC, Boyd ES, Semrau JD, Antholine WE, Han JI, Zahn JA, Boyd JM, de
493 la Mora AM, DiSpirito AA. 2003. The membrane-associated methane
494 monooxygenase (pMMO) and pMMO-NADH:quinone oxidoreductase complex from
495 *Methylococcus capsulatus* Bath. J Bacteriol 185:5755-64.

496 4. Elango N, Radhakrishnan R, Froland WA, Wallar BJ, Earhart CA, Lipscomb JD,
497 Ohlendorf DH. 1997. Crystal structure of the hydroxylase component of methane
498 monooxygenase from *Methylosinus trichosporium* OB3b. Protein Sc 6:556 - 568.

499 5. Fox BG, Hendrich MP, Surerus KK, Andersson KK, Froland WA, Lipscomb JD, Münck
500 E. 1993. Mössbauer, EPR, and ENDOR studies of the hydroxylase and reductase
501 components of methane monooxygenase from *Methylosinus trichosporium* Ob3b. J
502 Am Chem Soc 115:3688-3701.

503 6. Lipscomb JD. 1994. Biochemistry of the soluble methane monooxygenase. Ann Rev
504 Microbiol 48:371-399.

505 7. Colby J, Dalton H. 1978. Resolution of the methane monooxygenase of *Methylococcus*
506 *capsulatus* (Bath) into three components. Purification and properties of component
507 C, a flavoprotein. Biochem J 171:461 - 468.

8. Lieberman RL, Rosenzweig AC. 2005. Crystal structure of a membrane-bound metalloenzyme that catalyses the biological oxidation of methane. Nature 434:177-182.

9. Dalton H, Prior SD, Leak DJ, Stanley SH. 1984. Regulation and Control of Methane Monooxygenase. *In* Crawford RL, Hanson RS (ed), Microbial Growth in C1 Compounds. American Society for Microbiology, Washington, D.C.

10. Zahn JA, Bergmann DJ, Boyd JM, Kunz RC, DiSpirito AA. 2001. Membrane-associated quinoprotein formaldehyde dehydrogenase from *Methylococcus capsulatus* Bath. J Bacteriol 183:6832-6840.

11. DiSpirito AA, Kunz RC, Choi DW, Zahn JA. 2004. Electron flow during methane oxidation in methanotrophs., p 141-169. *In* Zannoni D (ed), Respiration in Archaea and Bacteria Kluwer Scientific, The Netherlands.

12. Picone N, Camp HJMOd. 2019. Role of rare earch elements in methanol oxidation. Curr Opin Chem Biol 49:39-44.

13. Anthony C. 1982. The Biochemistry of Methylotrophs. Academic Press, London.

14. Anthony C. 1992. The structure of bacterial quinoprotein dehydrogenases. Int J Biochem 24:29 - 30.

15. Williams PA, Coates L, Mohammed F, Gill R, Erskine PT, Coker A, Wood SP, Anthony C, Cooper JB. 2004. The atomic structure of methanol dehydrogenase from *Methylobacterium extorquens*. Biol Crystall D61:75-79.

16. Read J, Gill R, Dales SL, Cooper JB, Wood SP, Anthony C. 1999. The molecular structure of an unusual cytochrom c_2 determined at 2.0A; the cytochrome c_H from Methylobacterium extorques. Protein Sc 8:1232-1240.

17. DiSpirito AA, Lipscomb JD, Lidstrom ME. 1990. Soluble cytochromes from the marine methanotroph *Methylomonas* sp. strain A4. J Bacteriol 172:5360-7.

18. Vorholt JA. 2002. Cofactor-dependent pathways of formaldehyde oxidation in methylotrophic bacteria. Arch Microbiol 178:239-49.

19. Vorholt JA, Chistoserdova L, Lidstrom ME, Thauer RK. 1998. Distribution of tetrahydromethanopterin-dependent enzyme in methylotrophic bacteria and phylogeny of methenyl tetraphydromethopterin cyclohydrolases. J Bacteriol 180:5351 - 5756.

20. Vorholt JA, Chistoserdova L, Stolyar SM, Thauer RK, Lidstrom ME. 1999. Distribution of tetrahydromethanopterin-dependent enzymes in methylotrophic bacteria and phylogeny of methenyl tetrahydromethanopterin cyclohydrolases. J Bacteriol 181:5750-5757.

21. Jollie DR, Lipscomb JD. 1990. Formate dehyrogenase from *Methylosinus trichosporium* OB3b. Meth Enzymol 188:331 - 334.

22. Jollie DR, Lipscomb JD. 1991. Formate dehydrogenase from *Methylosinus trichosporium* OB3b. J Biol Chem 266:21853 - 21863.

23. Yoch DC, Chen CL, Hardt MG. 1990. Formate dehydrogenase from the methane oxidizer *Methylosinus trichosporium* OB3b. J Bacteriol 172:4456 - 4463.

24. Kits KD, Klotz MG, Stein LY. 2015. Methane oxidation coupled to nitrate reductio under hypoxia by gammaproteobacterium Methylomonas denitrificans, sp. nov. type strain FJG1. Environ Microbiol 17:3219-3232.

552 25. Sheng Y, Wang H, Liu Y, Zhu B, Li J, Yang Y, Qin W, Chen L, Wu X, Chistoserdova L,
553 Zhao F. 2020. Methane-dependent mineral reduction by aerobic methanotrophs
554 under hypoxia. Environ Sc Technol Lett doi:doi.org/10.1021/acs.estlett.0c00436.
555 26. Csaki R, Bodrossy L, Klem J, Murrell JC, Kovacs KL. 2003. Genes involved in the
556 copper-dependent regulation of soluble methane monooxygenase of *Methylococcus*
557 *capsulatus* (Bath): cloning, sequencing and mutational analysis. Microbiology
558 149:1785-1795.
559 27. Murrell JC, McDonald IR, Gilbert B. 2000. Regulation of expression of methane
560 monooxygenases by copper ions. Trend Microbiol 8:221-225.
561 28. Prior SD, Dalton H. 1985. Copper stress underlines the fundamental change in
562 intracellular location of the membrane monooxygenase in methane oxidizing
563 organisms: studies in batch and ontinuous culture. J Gen Microbiol 131:155 - 163.
564 29. DiSpirito AA, Semaru JD, Murrell JC, Gallagher WH, Dennison C, Vuilleumier S. 2016.
565 Methanobactin and the link between copper and bacterial methane oxidation.
566 Microbiol Mol Biol Rev 80:387-409.
567 30. El Ghazouani A, Basle A, Gray J, Graham DW, Firbank SJ, Dennison C. 2012.
568 Variations in methanobactin structure influences copper utilization by methane-
569 oxidizing bacteria. Proc Natl Acad Sci U S A 109:8400-4.
570 31. Semrau JD, DiSpirito AA, Obulisamy PK, Kang-Yun CS. 2020. Methanobactin from
571 methanotrophs: genetics, structure, function and potential applications. FEMS
572 Microbiol Lett 367:fnaa045.

573 32. Kim HJ, Graham DW, DiSpirito AA, Alterman MA, Galeva N, Larive CK, Asunskis D,
574 Sherwood PMA. 2004. Methanobactin, a copper-acquisition compound from
575 methane-oxidizing bacteria. Science 305:1612-1615.
576 33. Behling LA, Hartsel SC, Lewis DE, DiSpirito AA, Choi DW, Masterson LR, Veglia G,
577 Gallagher WH. 2008. NMR, mass spectrometry and chemical evidence reveal a
578 different chemical structure for methanobactin that contains oxazolone rings. J Am
579 Chem Soc 130:12604-5.
580 34. El Ghazouani A, Basle A, Firbank SJ, Knapp CW, Gray J, Graham DW, Dennison C.
581 2011. Copper-binding properties and structures of methanobactins from
582 *Methylosinus trichosporium* OB3b. Inorg Chem 50:1378-91.
583 35. Kenney GE, Goering AW, Ross MO, DeHart CJ, Thomas PM, Hoffman BM, Kelleher NL,
584 Rosenzweig AC. 2016. Characterization of methanobactin from *Methylosinus* sp.
585 SW4. J Am Chem Soc 138:11124 - 11127.
586 36. Krentz BD, Mulheron HJ, Semrau JD, DiSpirito AA, Bandow NL, Haft DH, Vuilleumier
587 S, Murrell JC, McEllistrem MT, Hartsel SC, Gallagher WH. 2010. A comparison of
588 methanobactins from *Methylosinus trichosporium* OB3b and *Methylocystis* strain SB2
589 predicts methanobactins are synthesized from diverse peptide precursors modified
590 to create a common core for binding and reducing copper ions. Biochemistry
591 49:10117-10130.
592 37. Gu W, Baral BS, DiSpirito AA, Semrau JD. 2017. An aminotransferase is responsible
593 for the deamination of the N-terminal leucine and required for formation of
594 oxazolone ring A in Methanobactin of *Methylosinus trichosporium* OB3b. Appl
595 Environ Microbiol 82:e01619-16.

596 38. Kim HJ, Graham DW, DiSpirito AA, Alterman MA, Galeva N, Larive CK, Asunskis D,
597 Sherwood PM. 2004. Methanobactin, a copper-acquisition compound from methane-
598 oxidizing bacteria. Science 305:1612-5.
599 39. Choi DW, Do YS, Zea CJ, McEllistrem MT, Lee SW, Semrau JD, Pohl NL, Kisting CJ,
600 Scardino LL, Hartsel SC, Boyd ES, Geesey GG, Riedel TP, Shafe PH, Kranski KA,
601 Tritsch JR, Antholine WE, DiSpirito AA. 2006. Spectral and thermodynamic
602 properties of Ag(I), Au(III), Cd(II), Co(II), Fe(III), Hg(II), Mn(II), Ni(II), Pb(II), U(IV),
603 and Zn(II) binding by methanobactin from *Methylosinus trichosporium* OB3b. J Inorg
604 Biochem 100:2150-61.
605 40. Baral BS, Bandow NL, Vorobev A, Freemeier BC, Bergman BH, Herdendorf T, Fuentes
606 N, Ellias L, Turpin E, Semrau JD, Di Spirito AA. 2014. Mercury binding by
607 methanobactin from *Methylocystis* strain SB2. J Inorgan Biochem 141:161 - 169.
608 41. Bandow NL. 2014. Isolation and binding properties of methanobactin from the
609 facultative methanotroph *Methylocystis* strain SB2. Ph.D. Iowa State University,
610 Ames, IA.
611 42. Lu X, Gu W, Zhao L, Fagan UHM, DiSpirito AA, Semrau JD, Gu B. 2017. Methylmercury
612 uptake and degradation by methanotrophs. Science Adv 3:e1700041.
613 43. Bandow N, Gilles VS, Freesmeier B, Semrau JD, Krentz B, Gallaghe W, McEllistrem
614 MT, Hartse SC, Cho DW, Hargrove MS, Heard TM, Chesner LM, Braunreiter KM, Cao
615 BV, Gavitt MM, Hoopes JZ, Johnson JM, Polster EM, Schoenick BD, A.M. U, DiSpirito
616 AA. 2012. Spectral and copper binding properties of methanobactin from the
617 facultative methanotroph *Methylocystis* strain SB2. J Inorgan Biochem 110:72 - 82.

618 44. Choi DW, Zea CJ, Do YS, Semrau JD, Antholine WE, Hargrove MS, Pohl NL, Boyd ES,
619 Geesey GG, Hartsel SC, Shafe PH, McEllistrem MT, Kisting CJ, Campbell D, Rao V, de la
620 Mora AM, Dispirito AA. 2006. Spectral, kinetic, and thermodynamic properties of
621 Cu(I) and Cu(II) binding by methanobactin from *Methylosinus trichosporium* OB3b.
622 Biochemistry 45:1442-53.
623 45. Baral BS. 2017. Methanobactin: Metal binding properties, physiological function and
624 biosynthesis. Ph.D. Iowa State University.
625 46. Zahao P, Astruc NLD. 2013. State of the art in gold nanoparticle synthesis. Coord
626 Chem Rev 257:638-665.
627 47. Chatwood LL, Müller J, Gross JD, Wagner G, S.J. L. 2004. NMR structure of the flavin
628 domain from soluble methane monooxygenase reductase from *Methylococcus*
629 *capsulatus* (Bath). Biochemistry 43:11983 - 11991.
630 48. Hayyan M, Hashim MA, AlNashef IM. 2016. Superoxide ion: generation and chemical
631 implications. Chem Rev 116:3029 - 3065.
632 49. Choi DW, Semrau JD, Antholine WE, Hartsel SC, Anderson RC, Carey JN, Dreis AM,
633 Kenseth EM, Renstrom JM, Scardino LL, Van Gorden GS, Volkert AA, Wingad AD,
634 Yanzer PJ, McEllistrem MT, de la Mora AM, DiSpirito AA. 2008. Oxidase, superoxide
635 dismutase, and hydrogen peroxide reductase activities of methanobactin from types
636 I and II methanotrophs. J Inorg Biochem 102:1571-80.
637 50. Latimer WM, Hildebrand JH. 1940. Reference Book of Inorganic Chemistry. The
638 Macmillan Co. , New York, NY, USA.
639 51. Carter P. 1971. Spectrometric determination of serum iron at the submicrogram
640 level with a new reagent (ferrozine). Anal Biochem 40:450-458.

641 52. Moody MD, Dailey HA. 1983. Aerobic ferrisiderophore reductase assay and activity
642 stain for native polyacrylamide gels. Anal Biochem 134:235-239.
643 53. Semau JD, DiSpirito AA, Obulisamy PK, Kang CS. 2020. Methanobactin from
644 methanotrophs: genetics, structure, function and potential applications. FEMS
645 Microbiol Lett 367:feaa045.
646 54. Milucka J, Kirf M, Lu L, Krupke A, Lam P, Littmann S, Kuypers MMM, Schubert CJ.
647 2015. Methane oxidation coupled to oxygenic photosynthesis in anoxic waters. ISME
648 J 9:1991-2002.
649 55. Oswald K, Milucka J, Brand A, Littmann S, Wehrll B, Kuypers MMM, Schubert CJ.
650 2015. Light-dependent aerobic methane oxidation reduces methane emissions from
651 seasonally stratified lakes. PLOS Ome 10.1371/journal.pone.0132574.
652 56. Oswald K, Jegge C, Tischer J, Berg J, Brand A, Miracle MR, Soria X, Vicente E,
653 Lehmann M, Zopfi J, Schubert CJ. 2016. Methanotrophy under versatile conditins in
654 water column of the ferruginous meromictic lake La Crus (Spain). Frount Microbiol
655 7:7:1762. doi: 10.3389/fmicb.2016.01762.
656 57. van Grinsven S, Damste JSS, Harrison J, Villanueva L. 2020. Impact of electron
657 acceptor availability on methane-influenced microorganisms in an enrichment
658 culture obtained from a stratified lake. Fount Microbiol 103389/micrb.2020.00715.
659 58. Gilman A, Fu Y, Hendershott M, Chu F, Puri AW, Smith AL, Pesecky M, Lieberman R,
660 Beck DAC. 2017. Oxygen-limited metabolism in the methanotroph
661 *Methylomicrobium buryatense* 5GB1C. PeerJ 5:e3945.
662 59. Amaral JA, Knowles R. 1995. Growth of methanotrophs in methane and oxygen
663 counter gradients. FEMS Microbiol Lett 216:215-220.

664 60. Henckel T, Roslev P, Conrad R. 2000. Effects of O_2 and CH_4 on presence and activity
665 of the indigenous methanotrophic community in rice field soil Microbiology 2:666-
666 679.
667 61. Lee HJ, Jeong SE, Kim PJ, Madsen EL, Jeon CO. 2015. High resolution depth
668 distribution of Bacteria, Archaea, methanotrophs, and methanogens in the bulk and
669 rhizosphere soils of a flooded rice paddy. Front, Microbiol
670 6:doi.org/10.3389/fmicb.2015.00639.
671 62. Choi DW, Bandow NL, McEllistrem MT, Semrau JD, Antholine WE, Hartsel SC,
672 Gallagher W, Zea CJ, Pohl NL, Zahn JA, DiSpirito AA. 2010. Spectral and
673 thermodynamic properties of methanobactin from gamma-proteobacterial methane
674 oxidizing bacteria: a case for copper competition on a molecular level. J Inorg
675 Biochem 104:1240-7.
676 63. Mandal M, Kawashima K, Saito K, Ishikita H. 2020. Redox Potential of the Oxygen-
677 Evolving Complex in Electron Transfer Cascade of Photosystem II. J Phys Chem Lett
678 11:249-255.
679 64. Vass I, Styring S. 1991. pH-Dependent Charge Equilibria between Tyrosine-D and
680 the S States in Photosystem II. Estimation of Relative Midpoint Redox Potentials.
681 Biochemistry 30:830-839.
682 65. Nicholls P, Fita I, Loewen PC. 2001. Enzymology and structure of catalases. Adv
683 Inorg Chem 51:51-106.
684 66. Apel K, Hurt H. 2004. Reactive oxygen species: metabolism, oxidative stress, and
685 signal transduction. Annu Rev Plant Biol 55:373-399.

686 67. Youngblut MD, Tsai C-L, Clark IC, Carlson HK, Magiaqui AP, Gau-Pan PS, Redford SA,
687 Wong A, Tainer JA, Coates JD. 2016. Perchlorate reductase is distinguished by active
688 site aromatic gate residues. J Biol Chem, 291:9190-9202.
689 68. Ettwig KF, Butler MK, Le Paslier D, Pelletier E, Mangenot S, Kuypers MM, Schreiber
690 F, Dutilh BE, Zedelius J, de Beer D, Gloerich J, Wessels HJ, van Alen T, Luesken F, Wu
691 ML, van de Pas-Schoonen KT, Op den Camp HJ, Janssen-Megens EM, Francoijs KJ,
692 Stunnenberg H, Weissenbach J, Jetten MS, Strous M. 2010. Nitrite-driven anaerobic
693 methane oxidation by oxygenic bacteria. Nature 464:543 - 548.
694 69. Bab-Dinitz E, Shmuely H, Maupin-Fulow J, Eichler J, Shaanan B. 2006. *Haloferax*
695 *volcanii* PitA: an example of functional interaction between Pfam chlorite dismutase
696 and antibiotic biosynthesis monooxygenase familes? Bioinformatics 22:671-675.
697 70. Whittenbury R, Phillips KC, Wilkinson JF. 1970. Enrichment, isolation and some
698 properties of methane-utilizing bacteria. J Gen Microbiol 61:205-18.
699 71. Bandow NL, Gallagher WH, Behling L, Choi DW, Semrau JD, Hartsel SC, Gilles VS,
700 Dispirito AA. 2011. Isolation of methanobactin from the spent media of methane-
701 oxidizing bacteria. Meth Enzymol 495:259-69.
702 72. Harris DC. 2007. Quantitative Chemical Analysis, 7th Ed. W.H. Freeman and
703 Company.
704
705

706

707 Table 1

708 Distribution of Au as Au^{3+} and Au^{0} following incubation of MB-SB2 and $HAuCl_4$. Reduction rate

709 where determined from samples were less than 100 percent reduction was observed.

$HAuCl_4$: MB-SB2 Ratio	**Time (min)**	**Percent**		**Reduction Rate (Au^{3+} reduced min^{-1})**
		Au^{3+}	**Au^{0}**	
0.9	30	0	100	-
2.25	30	0	100	-
9	30	8	92	0.27
14	30	11	89	0.41
19	30	59	41	0.26
9	60	0	100	-
14	60	0	100	-
19	60	10	90	0.28
19	360	0	100	-

710

711

712 **Figure Legends**

713 **Fig. 1.** Gold X-ray photoelectric spectra of MS-SB2 (**A**) at gold to MB-SB2 molar ratio of 14 to 1
714 after 30 min incubation (○) and (**B**) at gold to MB-SB2 molar ratio of 19 to 1 after
715 30 min incubation. Experimental results (circles) fit with CASA XPS software to four
716 Gaussian/Lorentzian curves, using two peaks for Au^{3+} (orange curves) and two
717 peaks for Au^{0} (blue curves). Gold 4f core electrons are spin-orbit split as $4f_{7/2}$ and
718 $4f_{5/2}$, with a splitting of 3.7 eV and area ratio of 4:3, so that only two peaks are
719 independently fit: the $4f_{7/2}$ peaks for Au^{3+} and Au^{0}. The $4f_{5/2}$ peaks' position and
720 area are determined by the spin-orbit splitting; those parameters and the peak
721 widths are fixed in the fitting program. Background used was a Shirley type.

722

723 **Fig. 2.** A. A. Kinetics of Au binding by MB-SB2 at 4°C. (A) Rate of $HAuCl_4$ binding to the
724 imidazolone (△) and oxazolone (○) rings of mb-SB2 at 4°C as measured from the
725 absorbance change at 386 nm and 341 nm, respectively. The rates for Au binding
726 >2000 sec^{-1}, and were set at 2000 sec^{-1} in the figure. B. Emission at 429nm from
727 SB2-MB following excitation at 341nm after the addition of 0 (—), 0.25 (—), 0.5
728 (—), 0.75 (—), or 2.25 (—) $HAuCl_4$ per MB-SB2.

729

730 **Fig. 3. A**. pH changes following the addition of $HAuCl_4$, to aqueous solutions (△)or aqueous
731 solution of 40 µM MB-SB2 (△). **B.** pH changes following the addition of $CuCl_2$ to
732 aqueous solutions (△) or aqueous solution of 40 µM MB-SB2 (○). **C.** pH changes

following the addition of KCl to aqueous solutions (△) or aqueous solution of 40 µM MB-SB2 (O).

Fig.4. Mass spectra of head space gas of a reaction mixture containing 2mM MB-SB2 in 97% $H_2{}^{18}O$ (A) and following the addition of 20mM $HAuCl_4$ (B), 20mM $CuCl_2$ (C),), 10mM $CuCl_2$ (D), 20mM KCl (E),), 20mM AgF (F), 20mM $FeCl_3$ (G),), 20mM $HgCl_2$ (H),), 20mM $NiCl_2$ (I), 20mM $CoCl_2$ (J).

Fig. 5. $^{18,18}O_2$ concentration in the head space of a reaction mixture containing 2 mM MB-SB2 plus 20mM $HAuCl_4$ (△) or 20mM $CuCl_2$ (O) in 97% $H_2{}^{18}O$ and following the addition of 7.3 mM of catalase.

Fig. 6. Iron reductase activity of MB-SB2 (A) and MB-OB3b (B). Absorption change at 562 nm of reaction mixtures containing 1mM ferrozine plus 10mM $FeCl_3$ (——),1mM ferrozine plus 23.4µM MB-SB (——), 1mM ferrozine plus 10mM $FeCl_3$ and either 5.8 (——), 11.6 (——), 17.4 (——) or 23.4 (——) µM MB-SB2 (A) or MB-OB3b (B). C. Aqueous 4M $FeCl_3$ solution (a) and a 4M $FeCl_3$ solution plus 20 mM MB-SB2 4 hours after the addition of MB-SB2.

Fig.7. Mass spectra of head space gas of a reaction mixture containing 2mM MB-OB3b in 97% $H_2{}^{18}O$ (A) and following the addition of 20mM $HAuCl_4$ (B), 20mM $CuCl_2$ (C), and 20mM AgF (D).

Fig. 8. $^{13}CO_2$ production by *M. trichosporium* OB3b wild type (WT), WT plus 25 µM $CuCl_2$, WT plus 5 µM MB-OB3b, and WT plus 25 µM $CuCl_2$ and 5 µM MB-OB3b incubated in an Anaerobic glove box for 3 days.

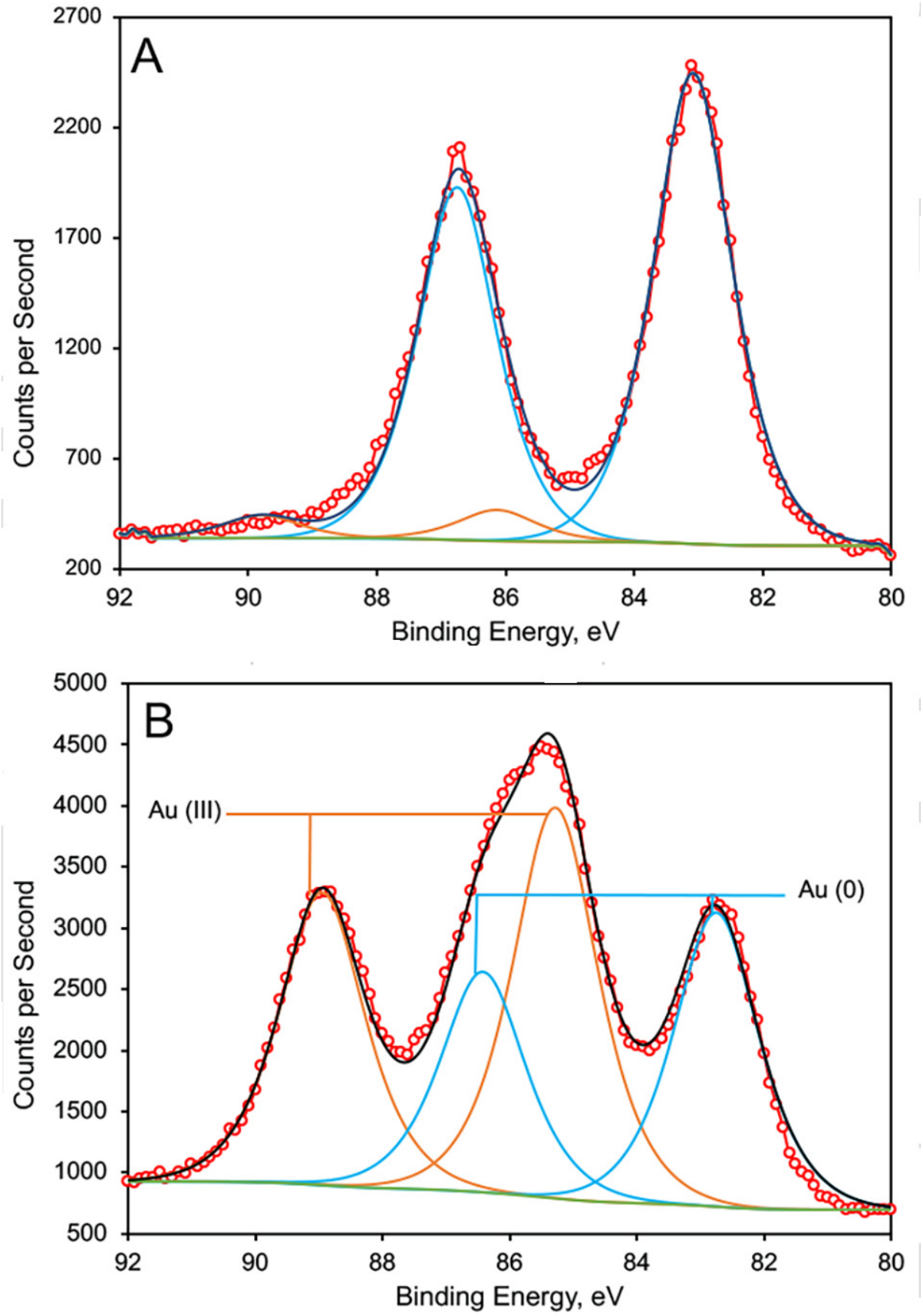

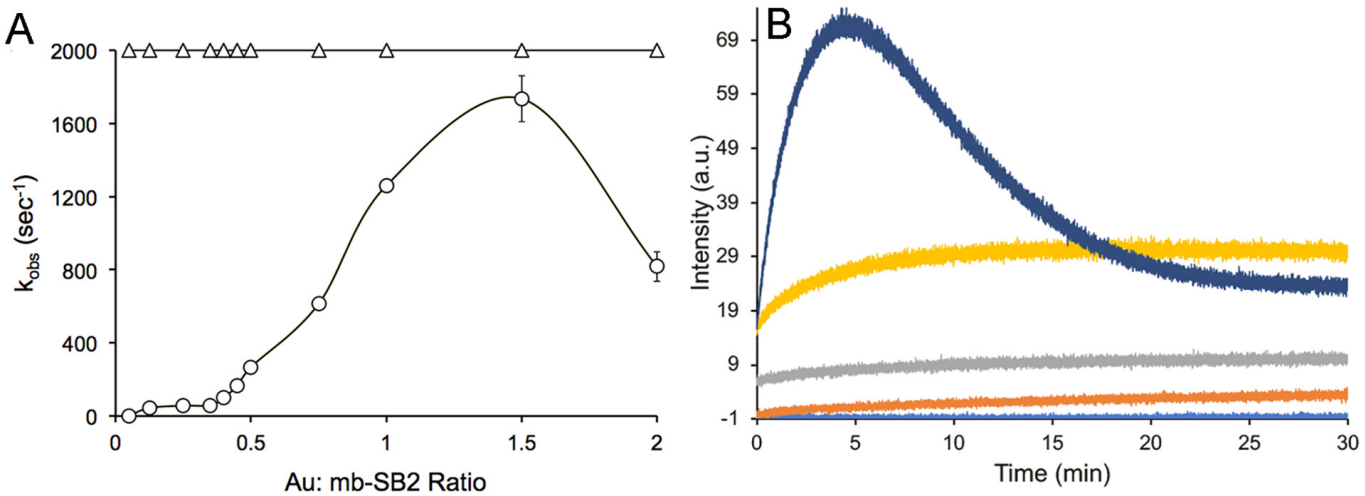

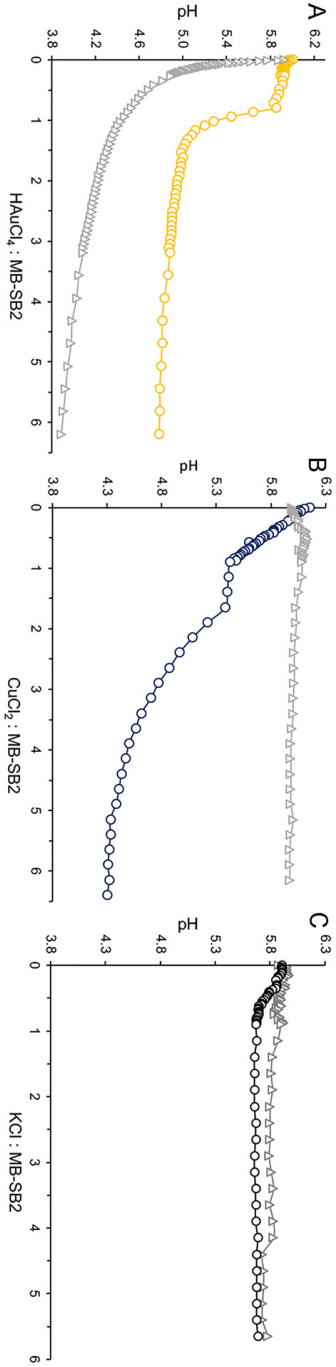

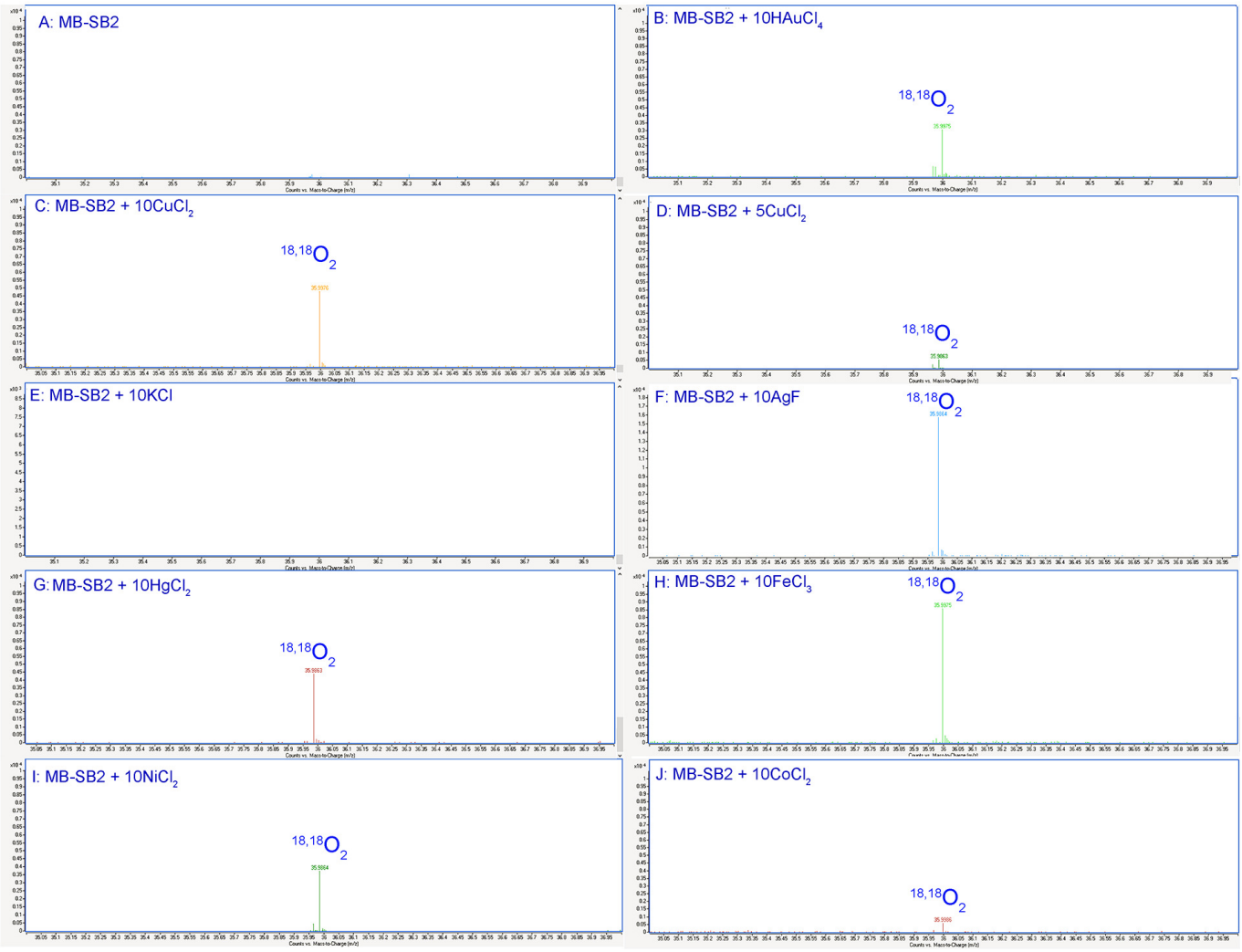

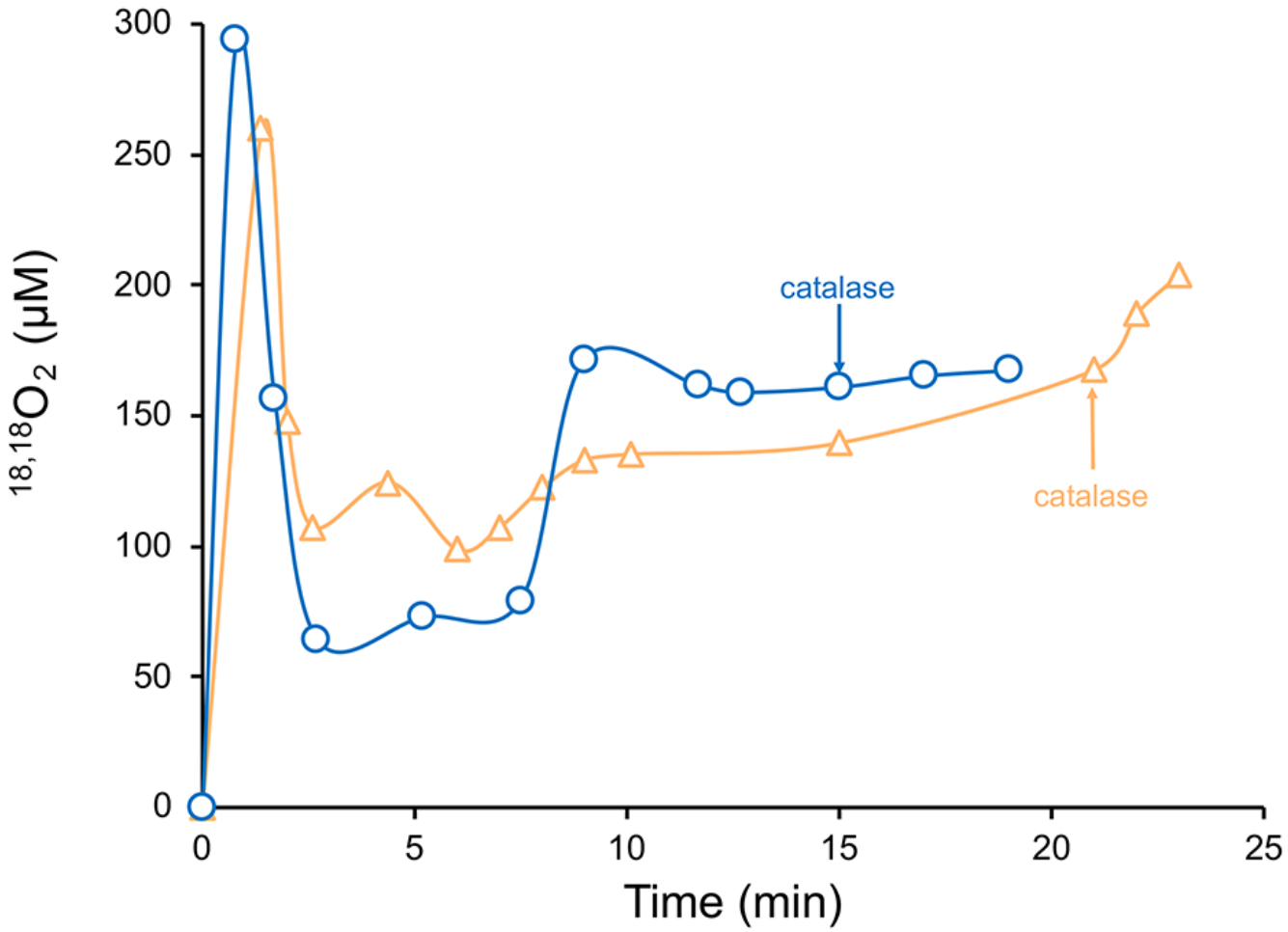

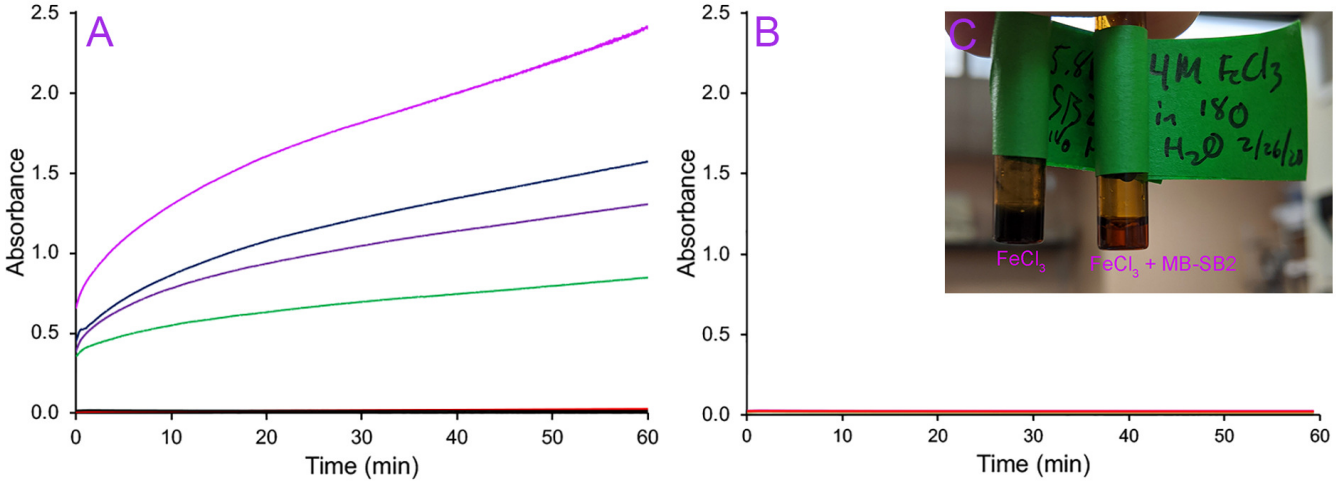

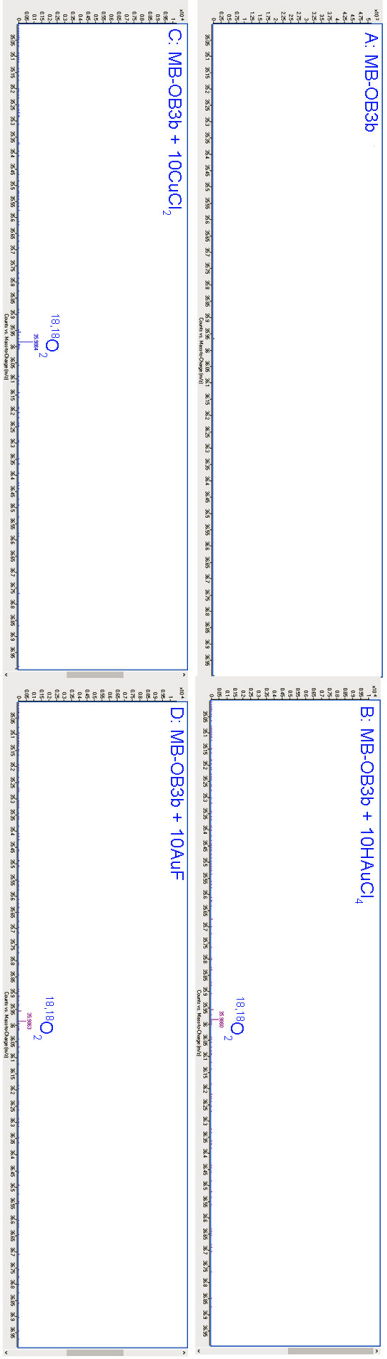

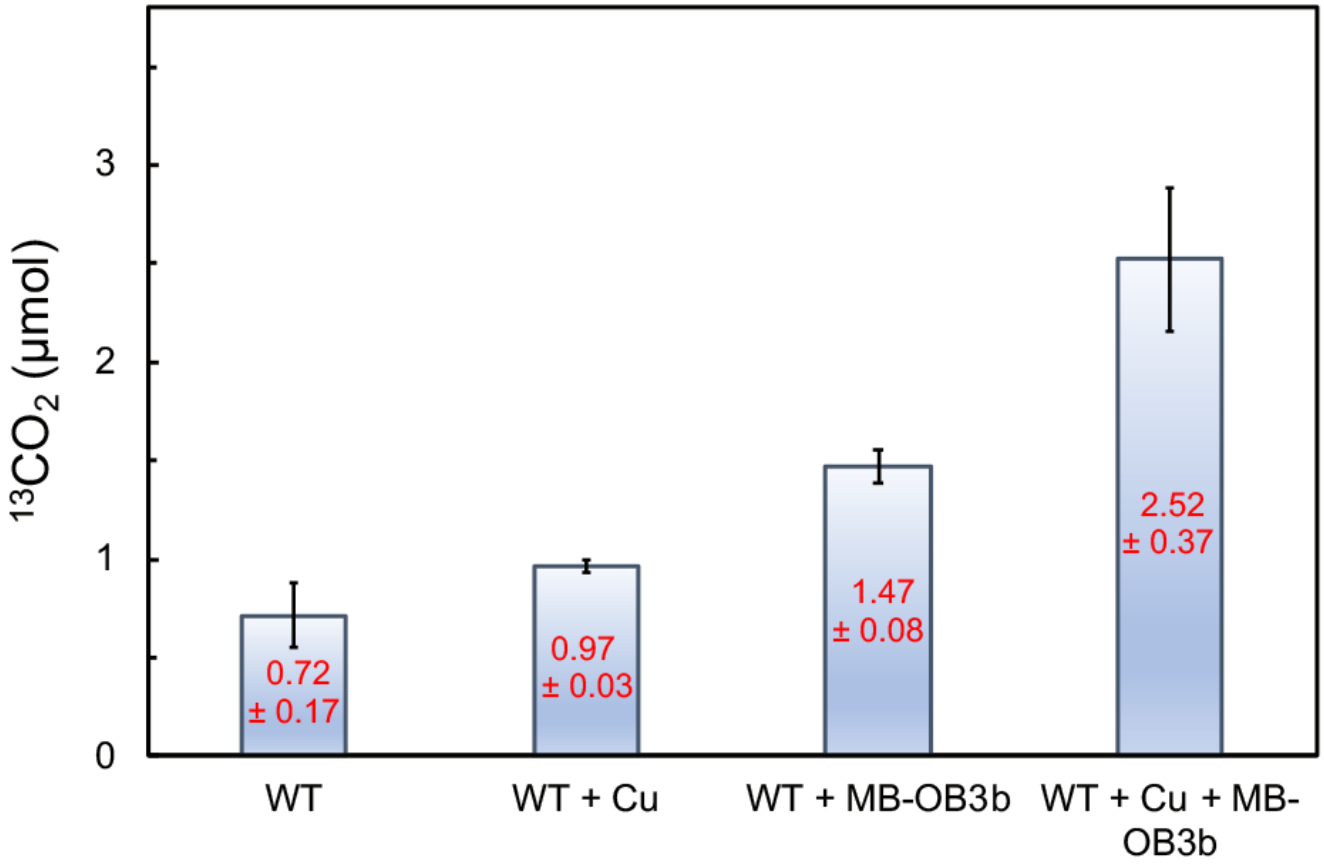

Table 1

Distribution of Au as Au^{3+} and Au^{0} following incubation of MB-SB2 and $HAuCl_4$. Reduction rate where determined from samples were less than 100 percent reduction was observed.

$HAuCl_4$: MB-SB2 Ratio	Time (min)	Percent		Reduction Rate (Au^{3+} reduced min^{-1})
		Au^{3+}	Au^{0}	
0.9	30	0	100	-
2.25	30	0	100	-
9	30	8	92	0.27
14	30	11	89	0.41
19	30	59	41	0.26
9	60	0	100	-
14	60	0	100	-
19	60	10	90	0.28
19	360	0	100	-